

# Multimodal Reasoning via Latent Refocusing

Jizheng Ma<sup>1,2</sup>, Xiaofei Zhou<sup>1,2†</sup>, Geyuan Zhang<sup>1,2</sup>, Yanlong Song<sup>1,2</sup>, Han Yan<sup>1,2</sup>

<sup>1</sup>Institute of Information Engineering, Chinese Academy of Sciences

<sup>2</sup>School of Cyber Security, University of Chinese Academy of Sciences

zhouxiaofei@iie.ac.cn

## Abstract

Chain of Thought (CoT) reasoning enhances logical performance by decomposing complex tasks, yet its multimodal extension faces a trade-off. The existing thinking with images paradigm is limited by the modality gap between vision and language, which hinders reliable extraction of reasoning relevant information from high dimensional visual data. Recent latent space reasoning method provides stronger multimodal representations, but it often lacks the ability to refocus on visual inputs and suffers from limited interpretability. To address these issues, we propose Latent Refocusing (LaRe), a novel multimodal reasoning paradigm that combines visual refocusing with rich latent representations, enabling iterative reasoning within the latent space. We further design a semantic augmentation training strategy that ensures the semantic structure of the latent space through joint alignment and reconstruction objectives. Experimental evaluations demonstrate that LaRe improves average accuracy by 9.4% compared to existing baselines while reducing the number of tokens required for inference by 16.5%. When scaled to a 7B-parameter Large Language Model backbone, LaRe achieves performance comparable to state-of-the-art models and outperforms larger-scale models on almost all benchmarks.

## 1 Introduction

The Chain of Thought (CoT) reasoning mechanism enhances the reasoning capabilities of large language models (LLMs) by decomposing complex problems through explicit intermediate steps (Wei et al., 2022; Zhou et al., 2024; Yao et al., 2023; OpenAI et al., 2024; Zhang et al., 2024; Wang et al., 2022; Brown et al., 2020; Minaee et al., 2024). With the rapid development of Multimodal Large

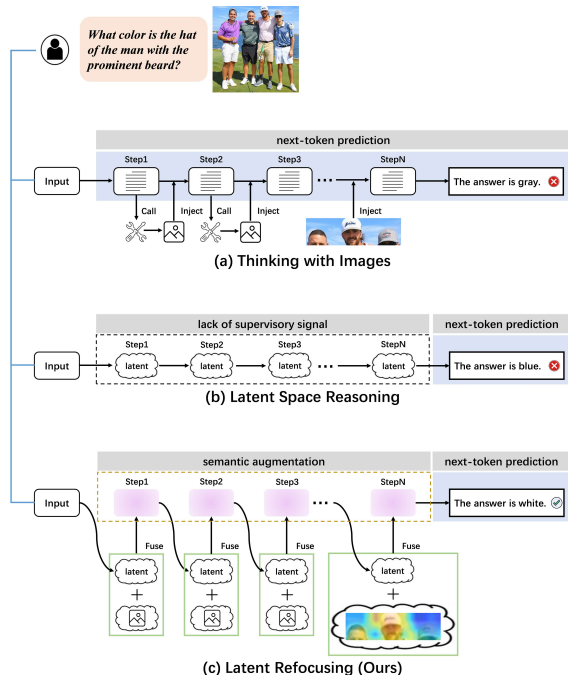


Figure 1: Illustrative comparison across thinking with images, latent space reasoning, and our proposed Latent Refocusing (LaRe) framework. LaRe performs refocusing within latent space, achieving more flexible reasoning.

Language Models (MLLMs) in recent years, extending Chain of Thought to multimodal scenarios has become increasingly important (Xu et al., 2023; Li et al., 2025d). This trend has given rise to multimodal reasoning as an emerging research direction that is gradually becoming an important technique for achieving artificial general intelligence (AGI) (Wang et al., 2025).

Currently, the predominant paradigm for multimodal reasoning is Thinking with Images (illustrated in Figure 1 (a)), which augments textual reasoning by injecting visual information into the reasoning chain (Fu et al., 2025; Gao et al., 2025). While effective, this paradigm is increasingly hitting a structural bottleneck: the modality gap. Vi-

<sup>†</sup>Corresponding author.

sual perception is high-dimensional and continuous, whereas linguistic reasoning is discrete and sequential. Directly forcing raw visual features into the textual manifold often leads to the extraction of task-irrelevant information or the loss of fine-grained spatial evidence, limiting the model’s ability to handle complex visual logic.

To mitigate this modality gap, a promising emerging direction is Latent Space Reasoning (illustrated in Figure 1 (b)) (Li et al., 2025c; Hao et al., 2024), which shifts the reasoning process from explicit tokens to latent representations. By performing inference within the hidden manifold, these methods can, in principle, preserve richer cross-modal information. However, current latent-based explorations are still in their infancy and lack the dynamic “refocusing” capability like the Thinking with Images paradigm. Most existing methods either compress reasoning into a static sequence (Su et al., 2025; Xu et al., 2025) or treat latent visual features as static initialization inputs (Li et al., 2025a). Moreover, prevailing training objectives are largely confined to conventional autoregressive language modeling leaving the latent space without effective supervisory signals and rendering latent representations a black box.

We observe a fundamental complementarity between these two paradigms. Thinking with Images offers dynamic reasoning but faces modality gaps, while Latent Space Reasoning mitigates gaps but lacks dynamic flexibility. To combine the strengths of both, we propose a Latent Refocusing (LaRe) paradigm, which unifies the dynamic advantages of Thinking with Images and the representational strengths of Latent Space Reasoning as depicted in Figure 1 (c). LaRe implements refocusing within the latent space via an iterative Latent Refocusing mechanism, which dynamically focuses on visual evidence based on the current reasoning state in the latent space.

Specifically, LaRe does not rely on explicit text or image tokens for reasoning. Instead it introduces a set of iteratively evolving latent representations. At each iteration a lightweight module refocuses on visual information conditioned on the current reasoning state and fuses it into the reasoning state to form latent tokens. These tokens then guide the next reasoning step producing an iterative thought process. The latent tokens inhabit a latent space that encodes the evolving intermediate reasoning states. To shape this space into a unified representation for multimodal semantics we design

a semantic augmentation training strategy. This strategy employs alignment and reconstruction objectives to induce a structured semantic layout in the latent space that is tailored for reasoning. The alignment objective ensures that the latent space encodes cross modal shared semantics while the reconstruction objective ensures that the latent space retains the fine grained visual and textual information required for reasoning. The contributions of this work are as follows:

- We propose Latent Refocusing, a novel multimodal reasoning paradigm that performs visual refocusing within the latent space. This design enables the model to carry out continuous optimization in the latent space, thereby achieving more flexible and efficient reasoning.
- We develop semantic augmentation training strategy tailored to latent space reasoning. These training objectives work jointly to induce a unified and semantically rich reasoning space.
- Experiments show that Latent Refocusing consistently outperforms strong baselines across multiple benchmarks. Qualitative analysis further reveals that the learned latent representations form semantically coherent structures and support interpretable latent semantic dynamics, offering valuable insights for future research on latent space reasoning.

## 2 Related Work

**Multimodal Reasoning.** Chain of Thought (CoT) reasoning was originally designed to augment the capabilities of Large Language Models (LLMs) through explicit reasoning steps (Wei et al., 2022) and has since been expanded into the multimodal domain (Wang et al., 2025). Early methodologies primarily relied on textual rationales (Zhang et al., 2023), though such approaches frequently struggle to capture fine grained spatial details. To bridge this gap, the *Thinking with Images* paradigm incorporates dynamic visual information into the reasoning process. For example, ReFocus (Fu et al., 2025) guides attention by highlighting structured regions, while Visual CoT (Rose et al., 2023) inserts image states into intermediate reasoning steps. Other methodologies such as Chain of Image (Meng et al., 2023) and VisualSketchpad (Hu et al., 2024) utilize auxiliary sketches for inference, whereas ICoT (Gao et al.,

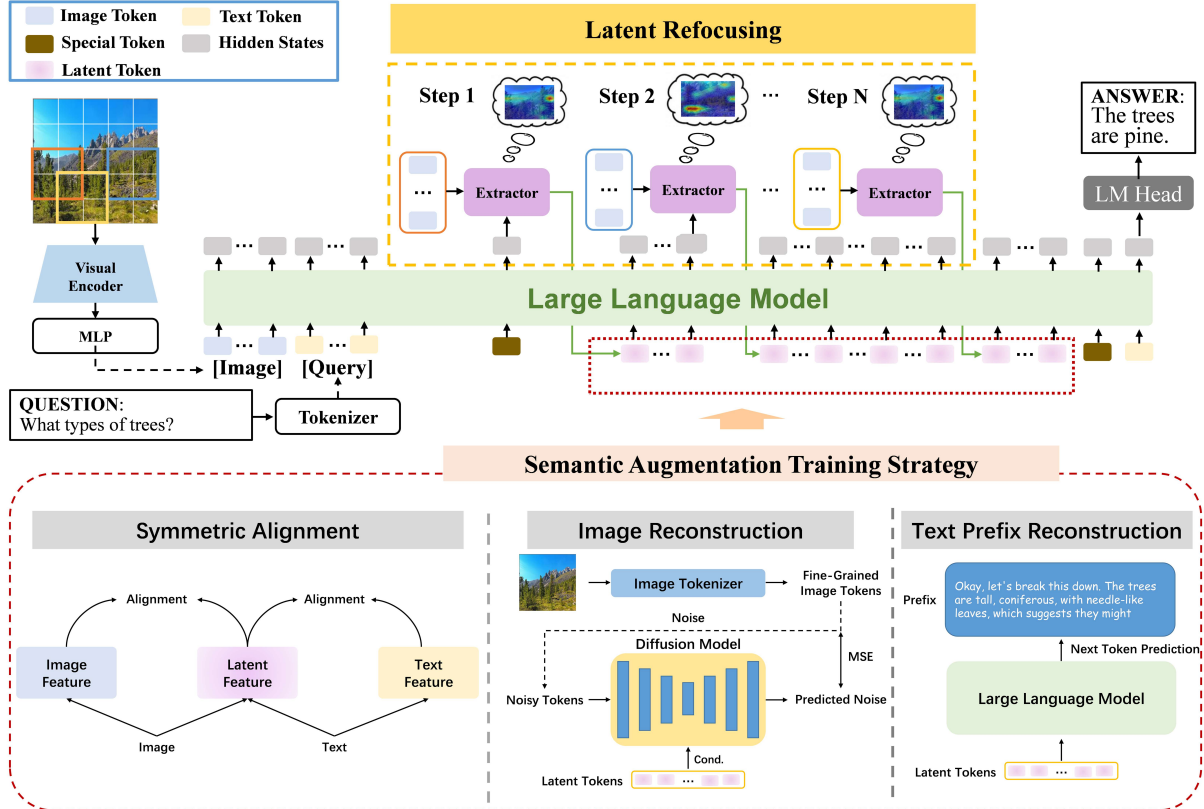


Figure 2: Overview of our proposed LaRe paradigm. The framework comprises Latent Refocusing (top), where the LLM and Extractor generate latent tokens by adaptively refocusing on visual evidence conditioned on reasoning states, and Semantic Augmentation (bottom), which employs Symmetric Alignment, Image Reconstruction, and Text Prefix Reconstruction to induce a semantically rich latent space for multimodal reasoning.

2025) constructs interleaved multimodal sequences. Although these methods improve reasoning fidelity, they remain constrained by the persistent modality gap between vision and language.

**Latent Space Reasoning.** Recent research trends have increasingly shifted toward latent space reasoning, which processes intermediate reasoning steps within the internal states of a model without explicit verbalization (Zhu et al., 2025; Li et al., 2025c). Existing works explore latent optimization at the token level (Tack et al., 2025; Sun et al., 2025; Gong et al., 2025) or the trajectory level (Hao et al., 2024; Shen et al., 2025a,b; Zhang et al., 2025b; Kong et al., 2025) while incorporating signal guided control mechanisms (Herel and Mikolov, 2024; Li et al., 2025b) and recurrent execution structures across layers (Saunshi et al., 2025; Mohtashami et al., 2025). Nevertheless, the majority of these approaches are restricted to the textual manifold. While several multimodal latent models have recently emerged, including MCOUT (Pham and Ngo, 2025), Mirage (Yang et al., 2025), and LVR (Li et al., 2025a), they frequently lack

effective back look mechanisms or rely on rigid supervision signals for regions of interest, thereby limiting their overall expressiveness and scalability.

### 3 Methodology

In this section, we present LaRe, a novel multimodal reasoning paradigm that performs refocusing within a shared latent space. LaRe consists of two core components: (1) an iterative Latent Refocusing mechanism that targets reasoning-relevant visual information through the introduction of dynamically evolving latent representations; and (2) a semantic augmentation training strategy designed to represent multimodal information within the latent space to facilitate the latent refocusing process.

#### 3.1 Latent Refocusing

LaRe endows the model with flexible multimodal reasoning capabilities through an iterative refocusing mechanism as illustrated in Figure 2. We model the reasoning process as a set of latent representations  $Z^{(k)}$  that evolve within the latent space, where  $k$  denotes the iteration step. These representations

encapsulate reasoning information and concentrate on the most relevant visual data.

Specifically, at each iteration step, we adaptively focus on and fuse reasoning-relevant visual information based on latent textual information to obtain latent tokens. Formally, the process of the  $k$ -th iteration step is expressed as follows:

$$\mathbf{H}_T^{(k)} = \mathbf{H}_{LLM}^{(k)}([\mathbf{V}_T; \mathbf{T}; \mathbf{Z}^{(1:k-1)}]), \quad (1)$$

$$\mathbf{Z}^{(k)} = \text{Extractor}(\mathbf{H}_T^{(k)}, \mathbf{V}_s). \quad (2)$$

In these equations,  $\mathbf{V}_T$  denotes the visual tokens obtained from the original image via a visual encoder and MLP,  $\mathbf{T}$  represents the text embeddings of the input query,  $\mathbf{V}_s$  signifies the local visual features obtained by a sliding window mechanism, and  $\mathbf{Z}^{(1:k-1)}$  constitutes the historical sequence of latent tokens generated in previous iterations.

During this process, the Large Language Model (LLM) functions as the decision hub. The LLM processes the concatenated input sequence and extracts hidden states, denoted as  $\mathbf{H}_{LLM}^{(k)}$ , to generate intermediate hidden representations  $\mathbf{H}_T^{(k)}$  from every layer. These representations encapsulate the textual reasoning information of the model at the current step as described by (Hao et al., 2024). Subsequently, the Extractor, acting as a lightweight semantic aggregation module, focuses on reasoning-relevant visual information from  $\mathbf{V}_s$  based on  $\mathbf{H}_T^{(k)}$  and fuses it into latent tokens.

**Sliding Window.** To mitigate computational overhead and visual redundancy, we employ an attention-based sliding window as a locality prior. By aggregating LLM attention weights into a saliency map  $\mathbf{A}_{2D}$  and applying  $w \times w$  sum-pooling, we extract local features  $\mathbf{V}_s$  from highly attended regions. This mechanism partitions the visual input into manageable candidates but inevitably retains distracting information. This limitation underscores the necessity for the subsequent Extractor to perform refined refocusing.

**Extractor.** The Extractor is a lightweight Transformer module designed to focus on task-relevant evidence from the redundant local features  $\mathbf{V}_s$  through an  $N$ -layer process. Each layer performs internal logic modeling followed by cross-modal refocusing, both stabilized by residual connections to preserve reasoning context. Starting with  $\mathbf{L}^{(0)} = \mathbf{H}_T^{(k)}$ , the update rules for the  $i$ -th layer and the final synthesis of latent tokens  $\mathbf{Z}^{(k)}$  are:

$$\mathbf{L}_{SA}^{(i)} = \text{Self-Attn}(\text{Norm}(\text{Linear}(\mathbf{L}^{(i-1)}))) + \mathbf{L}^{(i-1)}, \quad (3)$$

$$\mathbf{L}_{CA}^{(i)} = \text{Cross-Attn}(\text{Norm}(\mathbf{L}_{SA}^{(i)}), \mathbf{V}_s) + \mathbf{L}_{SA}^{(i)}, \quad (4)$$

$$\mathbf{Z}^{(k)} = \text{FFN}(\text{GLU}(\mathbf{L}_{CA}^{(N)})). \quad (5)$$

By employing the latent state as a query to probe  $\mathbf{V}_s$ , the Extractor extracts the precise visual signals required for the current reasoning step. The resulting  $\mathbf{Z}^{(k)}$  serves as a semantic carrier to drive the subsequent iteration of the large language model.

**Inference Phase.** After reaching the preset number of iterations  $K$ , we prepend and append the  $<|bot|>$  and  $<|eot|>$  special tokens to the latent sequence to delimit the boundaries of the continuous iteration, attach this sequence to the original image-text input, and then let the model generate text tokens autoregressively.

### 3.2 Semantic Augmentation

To induce a structured semantic layout in the shared latent space that is conducive to multi-step iterative reasoning, we employ a cooperative multi-objective training scheme during training, referred to as semantic augmentation.

**Symmetric Alignment.** To prevent semantic drift and ensure cross-modal consistency, we ground the latent tokens  $\mathbf{Z} \in \mathbb{R}^{B \times D}$  onto a shared multimodal manifold by aligning them with textual  $\mathbf{H}_R$  and visual  $\mathbf{V}_T$  representations, where  $\mathbf{H}_R$  represents the hidden states derived from explicit reasoning text tokens via the LLM. Specifically, we employ a contrastive learning objective to maximize the mutual information between these modalities. The alignment loss between  $\mathbf{Z}$  and  $\mathbf{H}_R$  is:

$$\mathcal{L}_{Z \leftrightarrow T} = -\frac{1}{B} \sum_{i=1}^B \log \frac{\exp(\mathbf{Z}_i \cdot \mathbf{H}_{R,i} / \tau)}{\sum_{j=1}^B \exp(\mathbf{Z}_i \cdot \mathbf{H}_{R,j} / \tau)}, \quad (6)$$

where  $\tau$  is a temperature hyperparameter. The total objective is  $\mathcal{L}_{\text{sym}} = \mathcal{L}_{Z \leftrightarrow T} + \mathcal{L}_{Z \leftrightarrow V}$ , where  $\mathcal{L}_{Z \leftrightarrow V}$  is computed analogously. This mechanism compels latent tokens to converge toward a structured semantic center, ensuring the extracted features are logically interpretable for the LLM.

**Reconstruction.** To prevent latent tokens from losing critical low-level details during latent space compression and refocusing, we introduce a multimodal reconstruction task as an additional regularization constraint. This objective requires the generated latent tokens to reconstruct fine-grained

visual representations and relevant explicit textual reasoning prefixes, thereby ensuring that the latent representations retain necessary evidentiary fidelity while possessing high-level semantics.

For visual reconstruction  $\mathcal{L}_{\text{img}}$ , we employ a denoising approach to reconstruct visual representations, as this method encourages the model to focus on the underlying data manifold (Karras et al., 2022; Chen et al., 2023). Specifically, this reconstruction objective is formalized using a denoising score matching loss:

$$\mathcal{L}_{\text{img}} = \mathbb{E} [|\epsilon - \epsilon_\theta(\sqrt{\bar{\alpha}_t} \mathbf{I}_z + \sqrt{1 - \bar{\alpha}_t} \epsilon, t, \mathbf{Z})|_2^2], \quad (7)$$

where  $t \sim \mathcal{U}(0, 1)$  is the sampled timestep,  $\mathbf{I}_z$  denotes the visual representations extracted by the sliding window and encoded by the Image Tokenizer,  $\epsilon \sim \mathcal{N}(0, \mathbf{I})$  represents the injected target noise,  $\bar{\alpha}_t$  is the predefined noise schedule coefficient, and  $\epsilon_\theta$  is a lightweight denoising U-Net (Ronneberger et al., 2015) conditioned on the latent tokens  $\mathbf{Z}$ .

For textual reconstruction  $\mathcal{L}_{\text{text}}$ , the goal is to ensure that latent tokens can be mapped back to the corresponding explicit reasoning tokens  $\mathbf{R}$ , maintaining the consistency of the logical chain:

$$\mathcal{L}_{\text{text}} = - \sum_{i=1}^{|\mathbf{R}|} \log P(r_i | \mathbf{Z}, r_{<i}). \quad (8)$$

The complete training objective combines these losses with the standard next-token prediction loss:

$$\mathcal{L}_{\text{ntp}} = - \sum_{i=1}^{|\mathbf{Y}|} \log P(y_i | \mathbf{V}_T, \mathbf{T}, \mathbf{Z}, y_{<i}), \quad (9)$$

$$\mathcal{L}_{\text{total}} = \mathcal{L}_{\text{ntp}} + \lambda_{\text{sym}} \mathcal{L}_{\text{sym}} + \lambda_{\text{img}} \mathcal{L}_{\text{img}} + \lambda_{\text{text}} \mathcal{L}_{\text{text}}, \quad (10)$$

where  $\lambda_{\text{sym}}$ ,  $\lambda_{\text{img}}$ ,  $\lambda_{\text{text}}$  are hyperparameters.

## 4 Experiments

### 4.1 Datasets and Evaluation

We evaluate LaRe on five benchmarks: MMBench (Liu et al., 2024b), MMStar (Chen et al., 2024), MMVP (Tong et al., 2024), ScienceQA (Lu et al., 2022), and POPE (Li et al., 2023), covering dimensions of comprehensive reasoning, visual perception, and hallucination detection. Evaluation metrics include answer accuracy (Acc.) and the number of tokens generated when producing a correct answer (# Tokens).

### 4.2 Baselines and Implementation Details

We compare LaRe with seven representative methods, including standard Chain of Thought reasoning methods that generate final answers through explicit step by step reasoning, text only multimodal reasoning approaches such as MM-CoT (Zhang et al., 2023) and CCoT (Mitra et al., 2024), Thinking with Images paradigms including ICoT (Gao et al., 2025) and CoF (Zhang et al., 2025a), and latent space reasoning paradigms including MCOUT (Pham and Ngo, 2025) and LVR (Li et al., 2025a).

All proposed and baseline methods are implemented on the Qwen2.5-0.5B and 1.5B Instruct backbones. To ensure fair comparison, we follow the LLaVA-v1.5 setup for pretraining and supervised fine tuning, while the post training stages of CoF and LVR adhere to their original settings. Detailed implementation details of LaRe are provided in the appendix B.

### 4.3 Main Results

We conducted a comprehensive evaluation of LaRe against multiple strong baseline methods and state-of-the-art multimodal models across five diverse benchmarks.

**Improved Accuracy.** As shown in Table 1, LaRe outperforms all comparison baselines at both the Qwen2.5-0.5B and 1.5B scales, achieving the highest accuracy across all five benchmarks. Across different backbone models and tasks, LaRe improves accuracy by approximately 10% compared with other methods. As reported in Table 2, when scaled to 7B parameters (including Qwen2.5-7B-Instruct (Qwen et al., 2025) and Vicuna-7B-v1.5 (Chiang et al., 2023) LLM backbones), LaRe-7B not only consistently surpasses larger models such LLaVA-NeXT-13B, but also attains performance comparable to GPT-4V on tasks including MMVP and ScienceQA, demonstrating the scalability of the proposed paradigm.

**Token Efficiency.** While improving accuracy, LaRe significantly reduces the number of tokens required for reasoning, with the average output length decreased by approximately 16.5%. This pronounced reduction in token usage not only implies lower computational overhead and inference cost, but also indicates that the Latent Refocusing mechanism can directly capture the key evidence required for reasoning at the level of latent semantics, effectively alleviating the redundancy of explicit

Table 1: Comparison to various multimodal reasoning baselines. The best results are **bolded**. \*Unlike LaRe and the other baseline methods, the post training of CoF and LVR follows their original settings.

Backbone	Method	MMBench		MMStar		MMVP		ScienceQA		POPE	
		Acc.	# Tokens								
Qwen2.5-0.5B-Instruct	Standard CoT	34.7	265.4	21.3	391.1	14.0	166.9	36.3	281.2	39.8	164.2
	MM-CoT (Zhang et al., 2023)	31.2	278.3	22.1	420.5	14.7	177.6	36.6	298.7	42.5	170.9
	CCoT (Mitra et al., 2024)	38.5	275.7	24.1	372.4	21.3	168.2	41.1	302.9	44.7	170.3
	ICoT (Gao et al., 2025)	39.4	253.8	23.6	<b>361.4</b>	28.2	165.7	40.4	294.2	45.1	161.2
	CoF* (Zhang et al., 2025a)	41.4	266.2	24.2	390.8	31.9	173.3	40.7	285.6	49.4	158.4
	MCOUT (Pham and Ngo, 2025)	34.9	265.3	19.9	405.4	26.2	167.6	32.4	283.3	42.3	157.7
	LVR* (Li et al., 2025a)	40.5	250.3	25.0	408.2	32.4	162.4	40.5	273.2	48.8	<b>126.5</b>
<b>LaRe (Ours)</b>		<b>51.2</b>	<b>225.1</b>	<b>32.2</b>	366.1	<b>36.2</b>	<b>153.0</b>	<b>42.3</b>	<b>256.9</b>	<b>52.6</b>	130.5
Qwen2.5-1.5B-Instruct	Standard CoT	43.2	395.2	21.6	521.7	16.6	227.1	38.3	426.2	44.2	179.5
	MM-CoT (Zhang et al., 2023)	43.4	430.7	22.5	590.9	18.8	229.0	41.6	433.8	44.1	172.0
	CCoT (Mitra et al., 2024)	47.0	425.6	27.3	596.2	31.4	235.8	43.1	440.3	50.8	182.3
	ICoT (Gao et al., 2025)	45.4	360.5	27.8	570.1	33.8	219.2	41.6	442.7	53.6	183.7
	CoF* (Zhang et al., 2025a)	53.7	330.4	32.1	534.5	40.2	222.3	43.3	445.4	53.6	186.1
	MCOUT (Pham and Ngo, 2025)	41.3	362.3	24.8	565.2	34.4	197.5	36.5	397.2	51.5	166.5
	LVR* (Li et al., 2025a)	51.2	340.7	30.4	595.3	39.9	208.4	42.4	370.9	53.1	173.4
<b>LaRe (Ours)</b>		<b>63.3</b>	<b>256.7</b>	<b>36.0</b>	<b>465.1</b>	<b>42.8</b>	<b>171.9</b>	<b>45.6</b>	<b>330.1</b>	<b>58.7</b>	<b>148.9</b>

Table 2: Performance of LaRe scaled to different 7B LLM backbones. The best results are **bolded** and the second best results are underlined.

Models	MMBench	MMStar	MMVP	POPE	ScienceQA
<b>LaRe-7B<sub>qwen</sub></b> (Qwen2.5-7B-Instruct)	73.4	<u>51.6</u>	<b>52.7</b>	<b>87.4</b>	<b>88.2</b>
<b>LaRe-7B<sub>vicuna</sub></b> (Vicuna-7B-v1.5)	64.6	47.3	<u>50.9</u>	82.6	80.1
<i>Literature reports</i>					
Chameleon-7B (Team, 2024)	16.7	31.7	18.7	48.8	45.0
LLaVA-NeXT-7B (Liu et al., 2024a)	64.2	33.3	36.7	–	42.2
DeepSeek-VL-7B (Lu et al., 2024)	73.2	37.1	40.7	85.8	<u>87.5</u>
Janus-pro-7B (Chen et al., 2025)	<b>79.2</b>	41.0	30.7	<b>87.4</b>	–
MiniCPM-V-2.6-8B (Yao et al., 2024)	70.3	51.4	46.0	86.7	86.9
Qwen-VL-Chat-9B (Bai et al., 2023)	61.8	34.5	21.0	85.3	–
LLaVA-NeXT-13B (Liu et al., 2024a)	70.0	43.9	37.3	86.2	85.2
GPT-4V (OpenAI, 2023)	<u>75.2</u>	<b>57.1</b>	50.0	75.4	–

reasoning.

#### 4.4 Qualitative Results

**Visualization of Each Iteration.** To intuitively illustrate the refocusing process of LaRe, Figure 3 presents a side by side visualization of the attention heatmaps produced by the Extractor module and the corresponding reasoning text trajectories across four consecutive iterations. We observe a highly consistent coevolution between the model’s visual focus regions and the process of textual evidence accumulation. In the first step, attention is primarily concentrated on the most salient foreground figures: the catcher and the umpire, which corresponds to the text marked in yellow. As reasoning progresses, the model refocuses on secondary regions: Step 2 localizes the batter and the players

inside the dugout, corresponding to the blue text. In Steps 3–4, the model further refocuses on relatively concealed figures in the background, such as staff members dressed in black (corresponding to the brown text) and individuals seated near the entrance of the dugout (corresponding to the purple text). Through this sequential refocusing, the model arrives at the correct answer, indicated by the green text. This progressive transition from coarse grained salient targets to fine grained background details clearly indicates that LaRe does not perform a static single pass recognition, but instead implements a structured multi step evidence focusing process. Crucially, a high degree of synchronization is observed between the attention heatmaps and the color coded reasoning text. Each segment of textual reasoning, such as “two staff members

Table 3: Ablation study of LaRe on Qwen2.5-1.5B-Instruct backbone. The results demonstrate that each component contributes critically to the full model’s performance and efficiency.

Methods	Acc.	# Tokens
LaRe	42.7	269.2
w/o Extractor	35.0 (-7.7)	311.5 (+42.3)
w/o Sliding Windows	38.7 (-4.0)	280.3 (+11.1)
w/o Symmetric Alignment	39.5 (-3.2)	276.9 (+7.7)
w/o Image Reconstruction	40.2 (-2.5)	274.0 (+4.8)
w/o Text Prefix Reconstruction	40.9 (-1.8)	263.6 (-5.6)

dressed in black watching the game,” corresponds to the visual region emphasized at the current step.

**From Latent to Images.** Through image reconstruction visualization in Figure 4, we show that a U-net fine-tuned for five epochs on ImageNet-1K (Deng et al., 2009) can successfully recover clear scenes from the latent sequences. This result provides direct evidence that the Latent Refocusing process indeed focuses on visual evidence throughout the entire reasoning process.

#### 4.5 Ablation Study

**Role of Each Module.** To verify the effectiveness of the core components in LaRe, we conduct ablation studies on the Qwen2.5-1.5B-Instruct backbone. As shown in Table 3, removing the Extractor results in the most severe performance degradation, with a score drop of 7.7% and a substantial increase in token consumption of 42.3%. This finding strongly demonstrates the decisive role of the Extractor in filtering visual noise and consolidating critical evidence into the latent space. The absence of the Sliding Window leads to a performance decrease of 4.0%, confirming the necessity of capturing local information through scanning for multimodal reasoning. Furthermore, ablations on the semantic augmentation strategy indicate that Symmetric Alignment and Image Reconstruction are crucial for maintaining structured semantics in the reasoning space, contributing performance gains of 3.2% and 2.5% respectively. Notably, although removing Text Prefix Reconstruction slightly reduces token usage, it still provides a positive contribution of 1.8% to the accuracy.

**Impact of Reasoning Steps.** The ablation study on the number of iterative steps (Figure 5) reveals a clear pattern of diminishing returns. Increasing the initial number of steps markedly improves per-

Table 4: Performance comparison of adaptive reasoning mechanisms using different convergence criteria.

Methods	Average Steps	Acc.	# Tokens
LaRe	4.0	42.7	269.2
+ Adaptive (Cosine)	5.9	42.6	265.1
+ Adaptive (L1 Distance)	2.8	42.0	279.8
+ Adaptive (L2 Distance)	2.9	42.5	270.5

formance and substantially reduces output length, validating the effectiveness of the iterative refocusing process. However, once the number of steps reaches a saturation threshold, both performance gains and output compression plateau. This finding indicates that the model can attain a stable reasoning state and offers guidance on the optimal number of steps to balance computational cost and reasoning effectiveness.

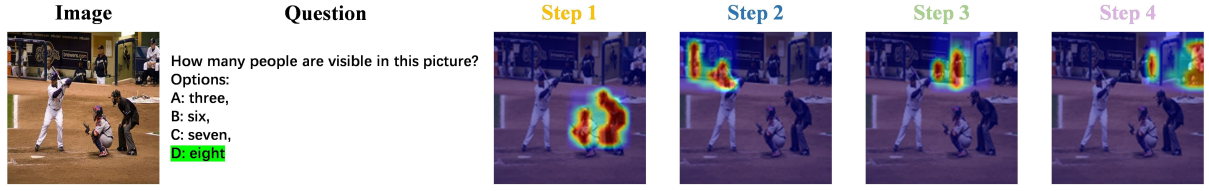
**Adaptive Reasoning Steps.** To enhance efficiency, we explore an adaptive stopping mechanism that determines reasoning termination based on the convergence of latent tokens. We assess this by tracking token evolution across iterations using cosine similarity, L1 distance, and L2 distance. As shown in Table 4, these metrics reveal a natural convergence trend where inter-step distances decrease monotonically as reasoning progresses. This observation validates the inherent stability of latent reasoning and corroborates the fixed-step ablation results in Fig. 5. However, the results highlight a clear efficiency-performance trade-off. While adaptive steps reduce computational overhead, they lead to performance degradation across most metrics. Future work will therefore investigate more refined stopping criteria to achieve truly efficient adaptive reasoning without sacrificing performance.

Table 5: Quantitative comparison on attention values. The results indicated that LaRe achieves higher values than LLaVA in both the mean and the median.

Statistic ( $\times 10^{-4}$ )	LLaVA	LaRe	P-value
Mean	4.47	10.84	$1.08 \times 10^{-7}$
25th Percentile	4.03	9.96	–
Median	4.44	10.76	$3.76 \times 10^{-9}$
75th Percentile	4.87	11.67	–
95th Percentile	5.54	13.03	–

#### 4.6 In-Depth Analysis

**Attention Analysis.** We compute the attention scores from the first generated token to all visual tokens on the MMStar dataset. We employ T-



#### Text-Only Response

Okay, I need to count how many people are visible in this picture. I will start by examining the central area of the image to identify the main figures involved in the action. I see a **catcher fully dressed in protective gear**, and directly behind the catcher stands an **umpire wearing dark-colored protective equipment**. Next to the catcher, there's a **batter at home plate wearing a white jersey, holding a bat and poised to swing**. Behind the batter, I can **see two players in the dugout**. I'll now scan the background to check for any additional people. Looking toward the dugout area, I notice **two staff members dressed in black watching the game**. I also observe more individuals inside the dugout—**one of them is clearly seated near the entrance**. After carefully counting each distinct individual I've identified, I conclude that there are a total of 8 visible people in the photo. Therefore, **the answer is 8**.

Figure 3: The evolution of attention in LaRe over four iterations and its alignment with the text-only reasoning trajectory.



Figure 4: Visual reconstructions from latent sequences. In each panel, the left image shows the original input (from the ImageNet-1K validation set), and the right image shows its reconstruction.

Table 6: Probing analysis results for semantic alignment of latent thoughts.

Backbone	Module	Classifier	Accuracy	
			Vision	Text
Qwen2.5-0.5B-Instruct	w/o Extractor	SVM	58.3	61.2
	with Extractor	SVM	94.7	95.1
	w/o Extractor	MLP	59.8	62.5
	with Extractor	MLP	96.2	96.8
Qwen2.5-1.5B-Instruct	w/o Extractor	SVM	59.1	62.8
	with Extractor	SVM	95.3	95.6
	w/o Extractor	MLP	60.2	63.4
	with Extractor	MLP	94.9	95.3
Llama-3.2-1B-Instruct	w/o Extractor	SVM	57.6	60.9
	with Extractor	SVM	93.8	94.2
	w/o Extractor	MLP	58.7	61.5
	with Extractor	MLP	93.5	94.0

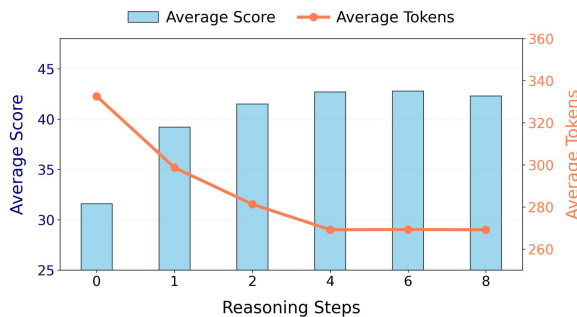


Figure 5: Impact of varying the number of reasoning steps on model performance and output efficiency.

**Probing Analysis.** To examine whether the latent tokens jointly encode linguistic reasoning and visual semantics, we conduct a probing analysis with two weak classifiers including SVM (Cortes and Vapnik, 1995) and MLP (Rumelhart et al., 1986). As shown in Table 6, LaRe achieves latent-vision and latent-text matching accuracy close to 95% across different backbone models. In contrast, removing the Extractor leads to a drop in probing accuracy to approximately 60%. These results provide strong evidence for the critical role of the Extractor, demonstrating its effectiveness in structuring cross-modal inputs into unified semantic representations within the latent space.

## 5 Conclusion

In this work, we introduced LaRe, a multimodal reasoning paradigm that bridges the modality gap by performing visual refocusing within a shared latent space. By decoupling the reasoning process from explicit token generation, LaRe addresses the limitations of traditional "Thinking with Images" while maintaining dynamic flexibility through its Latent Refocusing Mechanism. Our

test(Student, 1908) to compare the means and the Mann-Whitney U test(Mann and Whitney, 1947) to compare the medians of the two distributions. As shown in Table 5, LaRe achieves higher attention scores than LLaVA. This indicates that LaRe effectively guides the model to focus more on the input image, assigning greater weight to visual evidence, thereby enhancing its understanding of visual signals.

semantic augmentation training strategy further ensures that the latent space is semantically structured and grounded in both visual and textual evidence. Experimental evaluations across five benchmarks demonstrate that LaRe significantly outperforms current baselines in accuracy and reduces inference token consumption by an average of 16.5%. Scaling to 7B-parameter backbones further confirms its effectiveness and robustness. These results, supported by our probing and semantic analyses, highlight the potential of latent space reasoning as a more efficient and interpretable alternative for complex multimodal tasks.

## Limitations

A primary limitation of the current LaRe framework is its reliance on a predefined, static number of reasoning iterations  $K$ . While our empirical analysis identifies an optimal saturation threshold for performance, this "one-size-fits-all" approach does not account for the varying complexity across different multimodal tasks. For relatively straightforward visual queries, a fixed number of latent iterations may introduce redundant computational overhead and unnecessary latency. Conversely, for exceptionally intricate logical reasoning tasks, the model's performance may still be constrained by the preset iteration limit. Developing a dynamic halting mechanism, which allows the model to adaptively determine the required number of latent thoughts based on the evolving reasoning state—remains an important direction for further enhancing the efficiency and flexibility of the LaRe paradigm.

## Ethical Considerations

The datasets utilized in this study are publicly available benchmarks widely recognized in the research community. These datasets consist of images and textual annotations sourced from public domains and are used strictly for academic evaluation. To the best of our knowledge, all visual and textual data have been curated to ensure they do not contain Personally Identifiable Information (PII) or sensitive personal content. Our experimental procedures strictly adhere to the licensing agreements of the respective datasets and align with the ethical guidelines for responsible artificial intelligence research. Therefore, we believe that this work fully complies with the ethical standards of the conference.

## References

- Jinze Bai, Shuai Bai, Shusheng Yang, Shijie Wang, Sinan Tan, Peng Wang, Junyang Lin, Chang Zhou, and Jingren Zhou. 2023. Qwen-vl: A frontier large vision-language model with versatile abilities. *arXiv preprint arXiv:2308.12966*.
- Tom Brown, Benjamin Mann, Nick Ryder, Melanie Subbiah, Jared D Kaplan, Prafulla Dhariwal, Arvind Neelakantan, Pranav Shyam, Girish Sastry, Amanda Askell, and 1 others. 2020. Language models are few-shot learners. *Advances in neural information processing systems*, 33:1877–1901.
- Lin Chen, Jinsong Li, Xiaoyi Dong, Pan Zhang, Yuhang Zang, Zehui Chen, Haodong Duan, Jiaqi Wang, Yu Qiao, Dahua Lin, and 1 others. 2024. Are we on the right way for evaluating large vision-language models? *Advances in Neural Information Processing Systems*, 37:27056–27087.
- Minshuo Chen, Kaixuan Huang, Tuo Zhao, and Mengdi Wang. 2023. Score approximation, estimation and distribution recovery of diffusion models on low-dimensional data. In *International Conference on Machine Learning*, pages 4672–4712. PMLR.
- Xiaokang Chen, Zhiyu Wu, Xingchao Liu, Zizheng Pan, Wen Liu, Zhenda Xie, Xingkai Yu, and Chong Ruan. 2025. Janus-pro: Unified multimodal understanding and generation with data and model scaling. *arXiv preprint arXiv:2501.17811*.
- Wei-Lin Chiang, Zhuohan Li, Zi Lin, Ying Sheng, Zhanghao Wu, Hao Zhang, Lianmin Zheng, Siyuan Zhuang, Yonghao Zhuang, Joseph E. Gonzalez, Ion Stoica, and Eric P. Xing. 2023. Vicuna: An open-source chatbot impressing gpt-4 with 90%\* chatgpt quality.
- Corinna Cortes and Vladimir Vapnik. 1995. Support-vector networks. *Machine learning*, 20(3):273–297.
- Jia Deng, Wei Dong, Richard Socher, Li-Jia Li, Kai Li, and Li Fei-Fei. 2009. Imagenet: A large-scale hierarchical image database. In *2009 IEEE conference on computer vision and pattern recognition*, pages 248–255. Ieee.
- Xingyu Fu, Minqian Liu, Zhengyuan Yang, John Corring, Yijuan Lu, Jianwei Yang, Dan Roth, Dinei Florencio, and Cha Zhang. 2025. Refocus: Visual editing as a chain of thought for structured image understanding. *arXiv preprint arXiv:2501.05452*.
- Jun Gao, Yongqi Li, Ziqiang Cao, and Wenjie Li. 2025. Interleaved-modal chain-of-thought. In *Proceedings of the Computer Vision and Pattern Recognition Conference*, pages 19520–19529.
- Zhuocheng Gong, Jian Guan, Wei Wu, Huishuai Zhang, and Dongyan Zhao. 2025. Latent preference coding: Aligning large language models via discrete latent codes. *arXiv preprint arXiv:2505.04993*.

- Shibo Hao, Sainbayar Sukhbaatar, DiJia Su, Xian Li, Zhiting Hu, Jason Weston, and Yuandong Tian. 2024. Training large language models to reason in a continuous latent space. *arXiv preprint arXiv:2412.06769*.
- David Herel and Tomas Mikolov. 2024. Thinking tokens for language modeling. *arXiv preprint arXiv:2405.08644*.
- Yushi Hu, Weijia Shi, Xingyu Fu, Dan Roth, Mari Osendorf, Luke Zettlemoyer, Noah A Smith, and Ranjay Krishna. 2024. Visual sketchpad: Sketching as a visual chain of thought for multimodal language models. *Advances in Neural Information Processing Systems*, 37:139348–139379.
- Tero Karras, Miika Aittala, Timo Aila, and Samuli Laine. 2022. Elucidating the design space of diffusion-based generative models. *Advances in neural information processing systems*, 35:26565–26577.
- Aniruddha Kembhavi, Mike Salvato, Eric Kolve, Minjoon Seo, Hannaneh Hajishirzi, and Ali Farhadi. 2016. A diagram is worth a dozen images. In *Computer Vision–ECCV 2016: 14th European Conference, Amsterdam, The Netherlands, October 11–14, 2016, Proceedings, Part IV 14*, pages 235–251. Springer.
- Diederik P Kingma and Max Welling. 2013. Auto-encoding variational bayes. *arXiv preprint arXiv:1312.6114*.
- Deqian Kong, Minglu Zhao, Dehong Xu, Bo Pang, Shu Wang, Edouardo Honig, Zhangzhang Si, Chuan Li, Jianwen Xie, Sirui Xie, and 1 others. 2025. Scalable language models with posterior inference of latent thought vectors. *arXiv e-prints*, pages arXiv–2502.
- Bangzheng Li, Ximeng Sun, Jiang Liu, Ze Wang, Jialian Wu, Xiaodong Yu, Hao Chen, Emad Barsoum, Muham Chen, and Zicheng Liu. 2025a. Latent visual reasoning. *arXiv preprint arXiv:2509.24251*.
- Hengli Li, Chenxi Li, Tong Wu, Xuekai Zhu, Yuxuan Wang, Zhaoxin Yu, Eric Hanchen Jiang, Song-Chun Zhu, Zixia Jia, Ying Nian Wu, and 1 others. 2025b. Seek in the dark: Reasoning via test-time instance-level policy gradient in latent space. *arXiv preprint arXiv:2505.13308*.
- Jindong Li, Yali Fu, Li Fan, Jiahong Liu, Yao Shu, Chengwei Qin, Menglin Yang, Irwin King, and Rex Ying. 2025c. Implicit reasoning in large language models: A comprehensive survey.
- Yifan Li, Yifan Du, Kun Zhou, Jinpeng Wang, Wayne Xin Zhao, and Ji-Rong Wen. 2023. Evaluating object hallucination in large vision-language models. *arXiv preprint arXiv:2305.10355*.
- Zongxia Li, Xiyang Wu, Hongyang Du, Fuxiao Liu, Huy Nghiem, and Guangyao Shi. 2025d. A survey of state of the art large vision language models: Alignment, benchmark, evaluations and challenges. *Preprint*, arXiv:2501.02189.
- Haotian Liu, Chunyuan Li, Yuheng Li, and Yong Jae Lee. 2024a. Improved baselines with visual instruction tuning. In *CVPR*.
- Yuan Liu, Haodong Duan, Yuanhan Zhang, Bo Li, Songyang Zhang, Wangbo Zhao, Yike Yuan, Jiaqi Wang, Conghui He, Ziwei Liu, and 1 others. 2024b. Mmbench: Is your multi-modal model an all-around player? In *European conference on computer vision*, pages 216–233. Springer.
- Ilya Loshchilov and Frank Hutter. 2017. Decoupled weight decay regularization. *arXiv preprint arXiv:1711.05101*.
- Haoyu Lu, Wen Liu, Bo Zhang, Bingxuan Wang, Kai Dong, Bo Liu, Jingxiang Sun, Tongzheng Ren, Zhushou Li, Hao Yang, and 1 others. 2024. Deepseek-vl: towards real-world vision-language understanding. *arXiv preprint arXiv:2403.05525*.
- Pan Lu, Swaroop Mishra, Tanglin Xia, Liang Qiu, Kai-Wei Chang, Song-Chun Zhu, Oyvind Tafjord, Peter Clark, and Ashwin Kalyan. 2022. Learn to explain: Multimodal reasoning via thought chains for science question answering. *Advances in Neural Information Processing Systems*, 35:2507–2521.
- Henry B Mann and Donald R Whitney. 1947. On a test of whether one of two random variables is stochastically larger than the other. *The annals of mathematical statistics*, pages 50–60.
- Fanxu Meng, Haotong Yang, Yiding Wang, and Muhan Zhang. 2023. Chain of images for intuitively reasoning. *arXiv preprint arXiv:2311.09241*.
- Shervin Minaee, Tomas Mikolov, Narjes Nikzad, Meysam Chenaghlu, Richard Socher, Xavier Amatriain, and Jianfeng Gao. 2024. Large language models: A survey. *arXiv preprint arXiv:2402.06196*.
- Chancharik Mitra, Brandon Huang, Trevor Darrell, and Roei Herzig. 2024. Compositional chain-of-thought prompting for large multimodal models. In *Proceedings of the IEEE/CVF Conference on Computer Vision and Pattern Recognition*, pages 14420–14431.
- Amirkeivan Mohtashami, Matteo Pagliardini, and Martin Jaggi. 2025. Cotformer: A chain-of-thought driven architecture with budget-adaptive computation cost at inference. In *The Thirteenth International Conference on Learning Representations*.
- OpenAI. 2023. GPT-4V(ision) System Card.
- OpenAI, Aaron Jaech, Adam Kalai, Adam Lerer, Adam Richardson, Ahmed El-Kishky, Aiden Low, Alec Helyar, Aleksander Madry, Alex Beutel, Alex Carney, Alex Iftimie, Alex Karpenko, Alex Tachard Passos, Alexander Neitz, Alexander Prokofiev, Alexander Wei, Allison Tam, Ally Bennett, and 243 others. 2024. Openai o1 system card. *Preprint*, arXiv:2412.16720.

- Tan-Hanh Pham and Chris Ngo. 2025. Multimodal chain of continuous thought for latent-space reasoning in vision-language models. *arXiv preprint arXiv:2508.12587*.
- Qwen, An Yang, Baosong Yang, Beichen Zhang, Binyuan Hui, Bo Zheng, Bowen Yu, Chengyuan Li, Dayiheng Liu, Fei Huang, Haoran Wei, Huan Lin, Jian Yang, Jianhong Tu, Jianwei Zhang, Jianxin Yang, Jiaxi Yang, Jingren Zhou, Junyang Lin, and 24 others. 2025. [Qwen2.5 technical report](#). *Preprint*, arXiv:2412.15115.
- Alec Radford, Jong Wook Kim, Chris Hallacy, Aditya Ramesh, Gabriel Goh, Sandhini Agarwal, Girish Sastry, Amanda Askell, Pamela Mishkin, Jack Clark, and 1 others. 2021. Learning transferable visual models from natural language supervision. In *International conference on machine learning*, pages 8748–8763. PMLR.
- Robin Rombach, Andreas Blattmann, Dominik Lorenz, Patrick Esser, and Björn Ommer. 2022. High-resolution image synthesis with latent diffusion models. In *Proceedings of the IEEE/CVF conference on computer vision and pattern recognition*, pages 10684–10695.
- Olaf Ronneberger, Philipp Fischer, and Thomas Brox. 2015. U-net: Convolutional networks for biomedical image segmentation. In *International Conference on Medical image computing and computer-assisted intervention*, pages 234–241. Springer.
- Daniel Rose, Vaishnavi Himakunthala, Andy Ouyang, Ryan He, Alex Mei, Yujie Lu, Michael Saxon, Chinmay Sonar, Diba Mirza, and William Yang Wang. 2023. Visual chain of thought: bridging logical gaps with multimodal infillings. *arXiv preprint arXiv:2305.02317*.
- David E Rumelhart, Geoffrey E Hinton, and Ronald J Williams. 1986. Learning representations by back-propagating errors. *nature*, 323(6088):533–536.
- Nikunj Saunshi, Nishanth Dikkala, Zhiyuan Li, Sanjiv Kumar, and Sashank J Reddi. 2025. Reasoning with latent thoughts: On the power of looped transformers. *arXiv preprint arXiv:2502.17416*.
- Xuan Shen, Yizhou Wang, Xiangxi Shi, Yanzhi Wang, Pu Zhao, and Jiuxiang Gu. 2025a. Efficient reasoning with hidden thinking. *arXiv preprint arXiv:2501.19201*.
- Zhenyi Shen, Hanqi Yan, Linhai Zhang, Zhanghao Hu, Yali Du, and Yulan He. 2025b. Codi: Compressing chain-of-thought into continuous space via self-distillation. *arXiv preprint arXiv:2502.21074*.
- Student. 1908. The probable error of a mean. *Biometrika*, pages 1–25.
- DiJia Su, Hanlin Zhu, Yingchen Xu, Jiantao Jiao, Yuandong Tian, and Qinqing Zheng. 2025. Token assorted: Mixing latent and text tokens for improved language model reasoning. *arXiv preprint arXiv:2502.03275*.
- Yuchang Sun, Yanxi Chen, Yaliang Li, and Bolin Ding. 2025. Enhancing latent computation in transformers with latent tokens. *arXiv preprint arXiv:2505.12629*.
- Jihoon Tack, Jack Lanchantin, Jane Yu, Andrew Cohen, Ilia Kulikov, Janice Lan, Shibo Hao, Yuandong Tian, Jason Weston, and Xian Li. 2025. Llm pre-training with continuous concepts. *arXiv preprint arXiv:2502.08524*.
- Chameleon Team. 2024. Chameleon: Mixed-modal early-fusion foundation models. *arXiv preprint arXiv:2405.09818*.
- Shengbang Tong, Zhuang Liu, Yuexiang Zhai, Yi Ma, Yann LeCun, and Saining Xie. 2024. Eyes wide shut? exploring the visual shortcomings of multimodal llms. In *Proceedings of the IEEE/CVF Conference on Computer Vision and Pattern Recognition*, pages 9568–9578.
- Xuezhi Wang, Jason Wei, Dale Schuurmans, Quoc Le, Ed Chi, Sharan Narang, Aakanksha Chowdhery, and Denny Zhou. 2022. [Self-consistency improves chain of thought reasoning in language models](#). *Preprint*, arXiv:2203.11171.
- Yaoting Wang, Shengqiong Wu, Yuecheng Zhang, Shuicheng Yan, Ziwei Liu, Jiebo Luo, and Hao Fei. 2025. Multimodal chain-of-thought reasoning: A comprehensive survey. *arXiv preprint arXiv:2503.12605*.
- Jason Wei, Xuezhi Wang, Dale Schuurmans, Maarten Bosma, Fei Xia, Ed Chi, Quoc V Le, Denny Zhou, and 1 others. 2022. Chain-of-thought prompting elicits reasoning in large language models. *Advances in neural information processing systems*, 35:24824–24837.
- Peng Xu, Xiatian Zhu, and David A Clifton. 2023. Multimodal learning with transformers: A survey. *IEEE Transactions on Pattern Analysis and Machine Intelligence*, 45(10):12113–12132.
- Yige Xu, Xu Guo, Zhiwei Zeng, and Chunyan Miao. 2025. Softcot: Soft chain-of-thought for efficient reasoning with llms. *arXiv preprint arXiv:2502.12134*.
- Zeyuan Yang, Xueyang Yu, Delin Chen, Maohao Shen, and Chuang Gan. 2025. Machine mental imagery: Empower multimodal reasoning with latent visual tokens. *arXiv preprint arXiv:2506.17218*.
- Shunyu Yao, Dian Yu, Jeffrey Zhao, Izhak Shafran, Tom Griffiths, Yuan Cao, and Karthik Narasimhan. 2023. Tree of thoughts: Deliberate problem solving with large language models. *Advances in neural information processing systems*, 36:11809–11822.
- Yuan Yao, Tianyu Yu, Ao Zhang, Chongyi Wang, Junbo Cui, Hongji Zhu, Tianchi Cai, Haoyu Li, Weilin Zhao, Zhihui He, and 1 others. 2024. Minicpm-v: A gpt-4v level mllm on your phone. *arXiv preprint arXiv:2408.01800*.

Xintong Zhang, Zhi Gao, Bofei Zhang, Pengxiang Li, Xiaowen Zhang, Yang Liu, Tao Yuan, Yuwei Wu, Yunde Jia, Song-Chun Zhu, and 1 others. 2025a. Chain-of-focus: Adaptive visual search and zooming for multimodal reasoning via rl. *arXiv preprint arXiv:2505.15436*.

Xuan Zhang, Chao Du, Tianyu Pang, Qian Liu, Wei Gao, and Min Lin. 2024. Chain of preference optimization: Improving chain-of-thought reasoning in llms. *Advances in Neural Information Processing Systems*, 37:333–356.

Zhen Zhang, Xuehai He, Weixiang Yan, Ao Shen, Chenyang Zhao, Shuohang Wang, Yelong Shen, and Xin Eric Wang. 2025b. Soft thinking: Unlocking the reasoning potential of llms in continuous concept space. *arXiv preprint arXiv:2505.15778*.

Zhuosheng Zhang, Aston Zhang, Mu Li, Hai Zhao, George Karypis, and Alex Smola. 2023. Multi-modal chain-of-thought reasoning in language models. *arXiv preprint arXiv:2302.00923*.

Xiongtao Zhou, Jie He, Lanyu Chen, Jingyu Li, Haojing Chen, Víctor Gutiérrez-Basulto, Jeff Z Pan, and Hanjie Chen. 2024. Miceval: Unveiling multimodal chain of thought’s quality via image description and reasoning steps. *arXiv preprint arXiv:2410.14668*.

Rui-Jie Zhu, Tianhao Peng, Tianhao Cheng, Xingwei Qu, Jinfa Huang, Dawei Zhu, Hao Wang, Kaiwen Xue, Xuanliang Zhang, Yong Shan, Tianle Cai, Taylor Kergan, Assel Kembay, Andrew Smith, Chenghua Lin, Binh Nguyen, Yuqi Pan, Yuhong Chou, Zefan Cai, and 14 others. 2025. [A survey on latent reasoning](#). *Preprint*, arXiv:2507.06203.

## Appendix

---

### Algorithm 1 Latent Refocusing (LaRe)

---

**Require:** Input image  $I$ , text prompt  $T$ , number of reasoning steps  $K$ , special tokens  $\langle|\text{bot}|>$  &  $\langle|\text{eot}|>$

**Ensure:** Final answer  $\mathbf{Y}$

- 1:  $\mathbf{V}_T \leftarrow \text{MLP}(\text{VisualEncoder}(I))$   $\triangleright$  Extract global visual tokens
- 2:  $\mathbf{T} \leftarrow \text{Embed}(T)$   $\triangleright$  Project text to embedding space
- 3:  $\mathbf{V}_s \leftarrow \text{SlidingWindow}(\mathbf{V}_T, \mathbf{T})$   $\triangleright$  Obtain local candidate features via saliency
- 4:  $\mathbf{Z} \leftarrow \emptyset$   $\triangleright$  Initialize latent token sequence
- 5: **for**  $k = 1$  **to**  $K$  **do**
- 6:    $\mathbf{H}_T^{(k)} \leftarrow \text{LLM}_{\text{hidden}}([\mathbf{V}_T; \mathbf{T}; \mathbf{Z}])$   $\triangleright$  Extract current reasoning state from LLM
- 7:    $\mathbf{Z}^{(k)} \leftarrow \text{Extractor}(\mathbf{H}_T^{(k)}, \mathbf{V}_s)$   $\triangleright$  Refocus on  $\mathbf{V}_s$  and generate new latent token
- 8:    $\mathbf{Z} \leftarrow [\mathbf{Z}; \mathbf{Z}^{(k)}]$   $\triangleright$  Update the latent thought chain
- 9: **end for**
- 10:  $\text{Input}_{\text{final}} \leftarrow \begin{bmatrix} \mathbf{V}_T; \mathbf{T}; \langle|\text{bot}|>; \mathbf{Z}; \langle|\text{eot}|> \end{bmatrix}$   $\triangleright$  Concatenate all modalities
- 11:  $\mathbf{Y} \leftarrow \text{LLM}_{\text{generate}}(\text{Input}_{\text{final}})$   $\triangleright$  Autoregressive answer generation
- 12: **return**  $\mathbf{Y}$

---

## A Training Pipeline

We propose a four-stage training pipeline for LaRe. Details are provided in the below.

**Stage I: Vision–Language Alignment.** The primary goal of this stage is to establish conceptual alignment between visual and linguistic elements within the embedding space, enabling the LLM to interpret the entities presented in images. During this foundational phase, we focus on training the vision projection layers while keeping both the visual encoder and LLM backbone frozen.

**Stage II: Latent Alignment.** This stage aims to establish a semantically-grounded latent reasoning space by training the Extractor module to generate continuous thought representations that preserve essential visual information. We jointly optimize the Extractor parameters alongside the denoising U-Net while maintaining the pre-trained vision encoder and LLM backbone in a frozen state to ensure training stability.

**Stage III: Instruction Tuning.** In this stage, we fine-tune the model using instruction-tuning datasets to enhance its capability for instruction-following and dialogue. All model parameters undergo optimization with the exception of the visual encoder, which remains frozen throughout this process.

**Stage IV: Reasoning Fine-tuning.** This final stage focuses on integrating latent reasoning capabilities with downstream task performance. As in Stage III, all parameters with the exception of the visual encoder undergo fine-tuning.

The training objectives are structured progressively across stages. In Stage I, optimization relies exclusively on the autoregressive language modeling loss. Subsequent stages (II–IV) integrate the latent learning loss  $\mathcal{L}_{\text{total}}$ , formulated in Section 3, to enforce coherent latent reasoning.

## B Implementation Details

**Architecture of Extractor.** The Extractor module serves as the core component for executing iterative refocusing and adopts a Transformer-like architectural design. It consists of 2 iterative layers. In each layer, features are first preprocessed through a linear transformation, followed by a multi-head self-attention mechanism with 12 attention heads to model the evolution of internal reasoning dynamics. On this basis, a cross-attention mechanism, also configured with 12 heads, is applied over visual features to perform precise refocusing, thereby extracting evidence that is highly relevant to the current reasoning step. To ensure sufficient representational capacity, the hidden dimension of the Extractor is uniformly set to 1536. After completing the iterative process, the refined features are sequentially passed through a gated linear unit (GLU) and a feed-forward network (FFN), ultimately producing a latent representation that drives subsequent reasoning.

**Settings of Image Reconstruction.** The diffusion process employs a linear noise schedule defined by  $\beta_t \in [\beta_{\text{start}} = 1 \times 10^{-4}, \beta_{\text{end}} = 0.02]$  over  $T = 1000$  iterations. At each training step, a random timestep  $t \sim U(1, T)$  is sampled, and the input image  $x_0$  is corrupted as  $x_t = \sqrt{\bar{\alpha}_t}x_0 + \sqrt{1 - \bar{\alpha}_t}\epsilon$ , where  $\bar{\alpha}_t = \prod_{s=1}^t (1 - \beta_s)$ . The sampling process follows an iterative denoising procedure using the predicted noise and the reparameterization of the posterior distribution. We adopt

KL-16(Rombach et al., 2022) as the image tokenizer, which is a continuous VAE(Kingma and Welling, 2013) with a Kullback–Leibler (KL) divergence regularization term. The architecture of our denoising U-Net is illustrated in table 7.

**Other Hyperparameters.** The training process employs the AdamW optimizer (Loshchilov and Hutter, 2017) with  $\beta_1 = 0.9$ ,  $\beta_2 = 0.95$  and weight decay of 0.05 across all stages. For Stage I, we utilize a learning rate of  $1 \times 10^{-3}$  for the vision projection layers with the warmup ratio of 0.03, followed by cosine decay, training for one epoch with a global batch size of 256. Stage II employs a learning rate of  $2 \times 10^{-4}$  for the Extractor and reconstructor modules, training for one epoch with a reduced batch size of 128 to accommodate the additional computational requirements of the diffusion process. In Stages III and IV, all parameters except for the visual encoder are updated, while other hyperparameter settings remain identical to those in Stage II. As for the text prefix reconstruction, the prefix length is set to 32. The loss coefficients are set to  $\lambda_{sym} = 1.0$  for the symmetric alignment loss,  $\lambda_{img} = 0.9$  for the image reconstruction loss and  $\lambda_{text} = 0.9$  for the text prefix reconstruction loss, determined through grid search on the validation set. All models are trained using mixed precision (FP16) on 8 NVIDIA A100 80GB GPUs.

**Image Resolution Configurations** For image resolution configurations, all input images are resized to  $224 \times 224$  pixels to match the standard input requirements of the CLIP-ViT-L/14 visual encoder. This resolution yields 256 visual tokens after processing through the vision encoder (a  $16 \times 16$  grid of patch tokens). The diffusion-based reconstructor operates on latent representations with a feature map shape of  $[4, 28, 28]$ , corresponding to the compressed spatial dimensions while preserving essential visual information. During reconstruction evaluation, the output images are upsampled back to the original  $224 \times 224$  resolution for qualitative assessment.

**Data Decontamination Procedure.** To ensure the integrity of our evaluation and mitigate potential data contamination between the training set and the benchmark test sets, we implemented a rigorous two-stage decontamination process on the Vision-R1-cold dataset. First, we performed an exact match filtering based on textual question-answer pairs to explicitly remove

all samples originating from the official training splits of the AI2D(Kembhavi et al., 2016) and ScienceQA(Lu et al., 2022) benchmarks, which are known sources within Vision-R1-cold. Subsequently, to address more subtle, near-duplicate contamination at the image level, we employed a CLIP-ViT-L/14(Radford et al., 2021) model to compute image embeddings for all remaining Vision-R1-cold images and the images from the test splits of all our evaluation benchmarks. We then conducted a cross-dataset nearest-neighbor search. Any Vision-R1-cold sample whose image embedding had a cosine similarity of  $\geq 0.92$  with any test-set image embedding was identified as a semantic near-duplicate and removed. This conservative threshold was set to ensure the removal of visually and semantically highly analogous samples that could inflate performance metrics. In total, this procedure resulted in the removal of 4,479 samples from the original Vision-R1-cold dataset, thereby maximally ensuring that reported performance gains are attributable to our model’s improved reasoning capabilities rather than data leakage.

**Settings of Probing Analysis.** To rigorously evaluate whether the latent tokens  $\mathbf{Z}$  effectively encode joint linguistic reasoning and visual semantics, we conducted a comprehensive probing analysis following established methodologies in representation learning. The pooled latent vectors  $\mathbf{z}_{agg} = \phi_{pool}(\mathbf{Z})$ , textual rationale embeddings  $\mathbf{r} = \phi_{pool}(\mathbf{R})$ , and visual anchors  $\mathbf{v} = \phi_{pool}(\mathbf{V})$  were computed using the same hybrid pooling module (mean-max pooling) employed during training. All representations were subsequently projected to a 256-dimensional space via a lightweight, trainable linear layer and L2-normalized prior to classification to ensure scale-invariant comparison. For binary classification, positive pairs were constructed from matching (image, question) instances, while negative pairs were sampled in a balanced manner from three distinct strategies to prevent trivial solutions: (i) different-question/same-image, (ii) different-image/same-question, and (iii) random in-batch negatives. The final probing dataset comprised 1,000 labeled pairs (500 positive/500 negative) with a stratified 70/30 train/test split based on negative sampling type. We employed two distinct probe architectures: a Linear Support Vector Machine (SVM) with a linear kernel optimized via 5-fold cross-validation on the training set, and a

Table 7: U-Net configuration.

Parameter	Value
sample_size	img_size (input spatial size)
in_channels	self.channal (input feature channels)
out_channels	self.channal (output feature channels)
layers_per_block	3
block_out_channels	(96, 192, 384, 512)
down_block_types	(DownBlock2D, CrossAttnDownBlock2D, CrossAttnDownBlock2D, DownBlock2D)
up_block_types	(UpBlock2D, CrossAttnUpBlock2D, CrossAttnUpBlock2D, UpBlock2D)
cross_attention_dim	768
attention_head_dim	64
norm_num_groups	32

Table 8: Performance comparison with different sliding window sizes.

Methods	Avg. Score	Avg. Tokens	MMVP Accuracy
4 × 4	40.5	262.8	39.2
8 × 8	42.7	269.2	42.8
12 × 12	41.7	275.3	41.9

single-layer Multi-Layer Perceptron (MLP) implemented in PyTorch consisting of one hidden layer, optimized with Adam ( $\text{lr} = 1 \times 10^{-3}$ ) and early stopping based on validation loss.

## C Some Supplement Experiments Results

**Size of the Sliding Window.** We investigated the effect of sliding-window size on inference performance. As shown in Table 8, the choice of window size presents a trade-off between capturing fine-grained visual features and filtering out visual redundancy. The results indicate that overly small windows (e.g.,  $4 \times 4$ ), while maintaining low token consumption, lead to a marked drop in accuracy on benchmarks that heavily rely on visual perception (such as MMVP). This deterioration is likely caused by the reduced receptive field's inability to capture complete object structure or complex spatial interactions, thereby constraining the representational capacity of the latent space. Conversely, enlarging the window to  $12 \times 12$  produces a slight decrease in mean accuracy and increases the average number of tokens required for inference to 275.3. We attribute this performance decline primarily to the introduction of excessive task-irrelevant background noise with larger windows, which hampers the Extractor's ability to extract key evidence during the refocusing process. By contrast, the  $8 \times 8$  configuration attains the best balance across all evaluation metrics: it yields the highest perceptual accuracy on MMVP (42.8%) while preserving inference efficiency and providing

the most discriminative local visual signals. Accordingly, we adopt  $8 \times 8$  as the default window size.

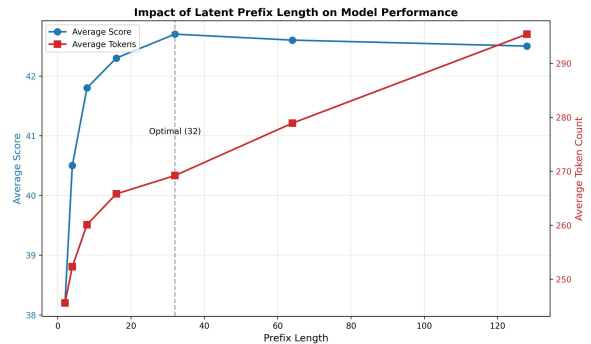


Figure 6: Effect of latent prefix length on model performance and efficiency. Performance improves with longer prefixes before saturating, while computational cost increases linearly. The optimal balance is achieved at 32 tokens.

**Impact of Prefix Length.** We investigate the sensitivity of LaRe to the length of the latent prefix used during training. As shown in Figure 6, model performance exhibits a clear pattern of improvement followed by saturation as prefix length increases from 2 to 128 tokens. Shorter prefixes (2-8 tokens) prove insufficient for capturing the complete reasoning trajectory, resulting in suboptimal performance. The optimal balance is achieved at our default setting of 32 tokens, where the model captures sufficient contextual information without introducing unnecessary redundancy. Extending the prefix beyond this point yields diminishing returns, with performance plateauing and computational cost increasing linearly. These findings validate our architectural choice and demonstrate that a moderate-length latent prefix effectively balances representational capacity with training efficiency.

## D Usage of LLMs

In this paper, LLMs were used for coding assistance and writing support. Specifically, they were employed to generate code snippets, debug existing scripts, and optimize algorithms, significantly accelerating the development cycle. For writing support, they were primarily utilized for proofreading the text and formatting *LaTeX* code.